

ORMNet: Object-centric Relationship Modeling for Egocentric Hand-object Segmentation

Yuejiao Su^a, Yi Wang^a, Lap-Pui Chau^{a,*}

^a*Department of Electrical and Electronic Engineering, The Hong Kong Polytechnic University, Hung Hom, Kowloon, Hong Kong SAR*

Abstract

Egocentric hand-object segmentation (EgoHOS) is a promising new task aiming at segmenting hands and interacting objects in egocentric images. Although EgoHOS has the potential to enable various applications, current methods struggle to achieve both high performance and end-to-end optimization simultaneously. Moreover, existing approaches fail to fully leverage hand cues to assist the interacting-object segmentation and overlook the coupled relationships between diverse interacting-object categories, resulting in performance deficiencies. To address these limitations, this paper proposes a novel Object-centric Relationship Modeling Network (ORMNet) to fulfill end-to-end and effective EgoHOS by modeling relationships between *hands and objects* as well as *objects and objects*. Specifically, a Hand-Object Relation (HOR) module is introduced to capture the correlation between hands and objects, which uses hand features to guide the network to extract more distinguishing interacting-object features. Besides, we find the coupling relations between diverse interacting-object categories and design the Object Relation Decoupling (ORD) strategy to disentangle them, emphasizing learning of the interaction between hands and objects and reducing the confusion of interacting-object classification. In-domain experiments show that ORMNet has notably exceptional segmentation performance compared with state-of-the-art methods, while out-of-domain experiments further exhibit its robust generalization capability. The project is available at <https://github.com/yuggiehk/ORMNet/>.

*Corresponding author.

Email addresses: yuejiao.su@connect.polyu.hk (Yuejiao Su), yi-eie.wang@polyu.edu.hk (Yi Wang), lap-pui.chau@polyu.edu.hk (Lap-Pui Chau)

Keywords: Egocentric perception, hand-object segmentation, cross-attention, relationship modeling

1. Introduction

The advancements in edge computing and computer vision [1, 2, 3] have engendered a growing interest in Head-Mounted Devices (HMD) such as the Apple Vision Pro [4] and Microsoft Hololens 2 [5]. Consequently, there is a rising trend in capturing abundant first-person view (FPV) or egocentric images and videos [6, 7]. Compared with data captured from a third-person view (TPV) or an exocentric perspective [8], egocentric data displays more detailed, intuitive, and clear actions and intentions of the HMD wearer, which is more conducive to analyzing human behavior and understanding how people interact with the environment. Notably, questions concerning the activities of individuals, such as “*What is this person doing?*” can be more comprehensively addressed in detail through the parsing of egocentric visual data. It is obvious that the hands of HMD wearers and the objects they are interacting with serve as pivotal cues in this analysis.

Therefore, to delve deeply into human behavior encoded within egocentric data at a fine-grained level, Zhang *et al.* [9] first proposed a new task, *i.e.*, Egocentric Hand-Object Segmentation (EgoHOS), which aims to perform pixel-level segmentation of hands and objects that are interacting with hands in egocentric images. This novel segmentation task enables a precise response to the query, “*Where are the left and right hands, and what objects are they interacting with?*” which can function as an essential algorithm serving as the foundation for various subsequent applications, such as augmented reality/virtual reality (AR/VR) [10, 11], medical assistive systems [12, 13], and embodied AI [14, 15].

The previous approaches for EgoHOS can be categorized into parallel and sequential methods. Specifically, some unified segmentation methods [9, 16, 17, 18, 19] can be directly used as parallel methods in this new task, which adopt an end-to-end framework to first extract image features and then simultaneously predict all categories of masks, as shown in Fig. 1 (a). However, due to the newly-emerging EgoHOS task,

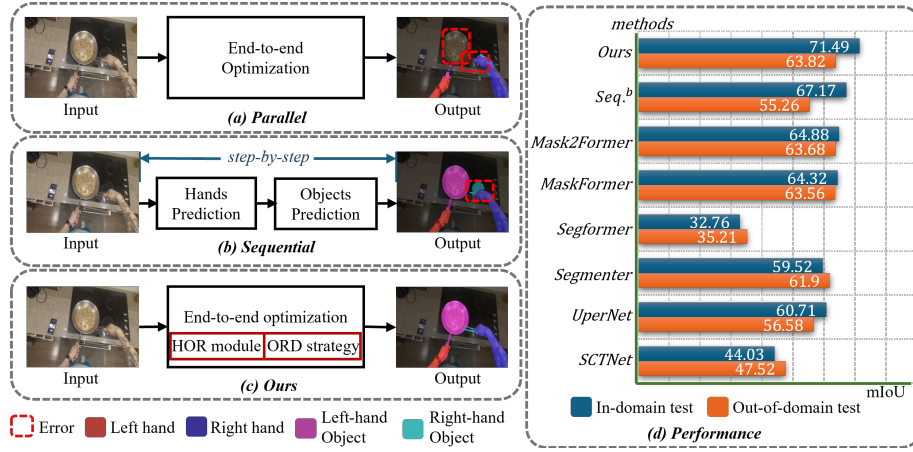


Figure 1: (a) parallel methods [9, 16, 17, 18, 19, 40], (b) sequential methods [9], and (c) our approach. Comparisons of segmentation performance (d) on the EgoHOS in-domain and out-of-domain test sets show that our ORMNet can achieve significant segmentation and generalization performance with end-to-end optimization by integrating the HOR module and ORD strategy.

applying such generic segmentation methodologies directly to this task lacks targeted design of relation modeling, resulting in suboptimal effectiveness. In contrast to parallel methods, sequential approaches [9] are specially designed to form a step-by-step prediction scheme for hands and interacting objects, *i.e.*, the input of the latter step to predict the objects’ masks necessitates the previous step’s output for predicting hands, as depicted in Fig. 1 (b). Although the effectiveness of sequential methods surpasses that of parallel methods, they are unable to achieve end-to-end optimization, which reduces the efficiency of the network. Therefore, achieving both high performance and end-to-end optimization in this new EgoHOS task remains an unresolved issue.

Furthermore, regardless of variations in interactions and environments, it is easier to recognize hands in egocentric images by identifying the shape and texture [20, 7]. Conversely, the segmentation of interacting objects presents significant challenges due to the reliance on discerning interaction with hands rather than visual features. Therefore, the dominant role of hands in the EgoHOS task underscores the benefit of incorporating hands to assist in predicting interacting objects. However, as mentioned above, parallel methods [9, 21, 22] treat hands and interacting objects as completely indepen-

dent categories for prediction, while sequential methods [9] use predicted hand masks as input for interacting-object segmentation. Both approaches fail to subtly and explicitly model the dominance of hands in predicting interacting objects, thereby leading to performance deficiencies.

In addition, the EgoHOS task requires the prediction of three types of interacting objects determined by the hand(s) they interact with, namely, left-hand objects, right-hand objects, and two-hand objects, as described in detail in Sec. 3.1. We observe that the two-hand object encompasses attributes of both the left- or right-hand object because they are interacting with both left- and right-hand simultaneously. However, most existing parallel and sequential approaches treat different types of interacting objects as separate, which requires the network to learn “whether the object is interacting with both hands at the same time,” introducing additional confusion into the training process and resulting in inaccurate results.

To address the shortcomings of the existing methods above, this paper proposes a novel **Object-centric Relationship Modeling Network** (ORMNet) to model the relationships between “*hands and objects*” as well as “*objects and objects*”, which can achieve end-to-end optimization with significant performance, as shown in Fig. 1 (c). On the one hand, we propose the Hand-Object Relation (HOR) module to establish the correlation between the features of the hand and interacting objects. The core underlying concept involves leveraging hand features as prior knowledge and employing hand-guided attention to extract more representative interacting-object features. On the other hand, based on the observations about interacting objects, we introduce a novel Object Relation Decoupling (ORD) strategy to disentangle the interrelationships among diverse interacting-object categories. This strategy restricts the prediction of the left- and right-hand objects exclusively during training, and another type of object (two-hand objects) is generated through an ingenious and pure mathematical *intersection* operation during inference. This strategy can help the algorithm emphasize the interaction and reduce the confusion of the algorithm about the interacting-object classification during learning. Experimental results on in-domain and out-of-domain test sets demonstrate the state-of-the-art performance of ORMNet along with robust generalization capabilities, as shown in Fig. 1 (d).

The contributions of this paper are as follows:

- This paper introduces a novel ORMNet for the EgoHOS task, achieving state-of-the-art segmentation performance while fulfilling end-to-end optimization.
- To take full advantage of the prominence of hand features, ORMNet incorporates the HOR module to model the relationship between hands and interacting objects, helping the network extract more representative object features.
- Based on the observed relation between various interacting-object categories, an innovative ORD strategy is proposed to decouple them, decreasing the concentration on classification and emphasizing interaction learning of the algorithm.
- The thorough experimental results demonstrate that the proposed ORMNet achieves exceptional performance and manifests robust generalization capabilities.

2. Related Work

This section mainly introduces the related work of this paper. Since the EgoHOS task is strongly related to Egocentric Hand-Object Interaction (EgoHOI), we will first introduce EgoHOI (Sec. 2.0.1) and then refine to EgoHOS (Sec. 2.0.2).

2.0.1. Egocentric Hand-Object Interaction

Egocentric images and videos offer a clear window into how humans physically engage with their surrounding environment and the objects using their hands. In recent years, the interpretation and analysis of egocentric visual data have earned increasing attention from the research community, especially in the field of Egocentric hand-object interaction (EgoHOI) [23, 24, 25] due to the release of various large-scale datasets [26, 24, 27, 28, 29].

Aiming to solve the EgoHOI task, certain efforts [30] used additional multi-modality information, such as gaze [31] and text [32, 33] cues, to enhance the learnable representations. Furthermore, self-supervised diagrams [34] were developed to effectively leverage the underlying visual information. Although egocentric visual data is inherently far more limited in quantity compared to the abundant third-person perspective

(TPV) data, some works [35, 36] proposed to learn the joint representations and transfer the view-agnostic knowledge from TPV to FPV. However, the data requirements are strict, time-consuming, and labor-intensive, which needs videos capturing the same action from different perspectives. In addition, EgoHOI can be utilized as a basic algorithm to perform other tasks, such as action recognition [20, 37, 38] and action anticipation [39]. While many transformer-based approaches have made breakthrough progress on the EgoHOI task, the sole prediction of bounding boxes around the interacting objects lacks the granularity of fine-grained analysis.

2.0.2. Egocentric Hand-Object Segmentation

Different from EgoHOI, EgoHOS is a novel problem proposed by Zhang *et al.* [9] to perform fine-grained pixel-level segmentation for hands and interacting objects. The final prediction output encompasses a set of categories, including the left hand, right hand, left-hand objects, right-hand objects, and two-hand objects. Furthermore, the authors also proposed different types of methods in their work, including parallel methods and sequential methods.

Parallel methods. Some general segmentation methods [9, 16, 17, 18, 19, 40] can be directly used as parallel methods to perform EgoHOS task. These methods take egocentric images as input, and directly obtain predictions of all categories after feature extraction and mask generation, as shown in Fig. 1 (a). Although these methods can complete the EgoHOS task in an end-to-end manner, they are not effective due to the lack of task-specific design.

Sequential methods. Zhang *et al.* proposed a series of sequential methods [9] tailored for the EgoHOS task, as shown in Fig. 1 (b). Taking the egocentric image as input, these step-by-step sequential methods first segment the left and right hands. After that, the segmented left- and right-hand masks are concatenated to the input image to perform the mask prediction of interacting objects. Although sequential methods achieve higher segmentation performance than the parallel method, the step-by-step process is unable to achieve end-to-end optimization, which limits the applications in the real world.

In addition, both parallel and sequential methods inadequately explore the relation-

ship between hands and interacting objects, which does not emphasize the leading role of the hand [20] in the EgoHOS task, thereby degrading the segmentation performance. Finally, parallel and sequential methods regard the different categories of interacting objects as independent and ignore the potential relationships between them, causing unnecessary confusion in classifying the interacting-object categories. Unlike the previous parallel and sequential methods, the proposed ORMNet can achieve end-to-end optimization with high accuracy due to the relationship modeling between “hands and objects” as well as “objects and objects,” as shown in Fig. 1 (c).

3. Methodology

This section introduces the proposed ORMNet in detail from top to bottom, including task description (in Sec. 3.1), overall architecture (in Sec. 3.2), HOR module (in Sec. 3.3), ORD strategy (in Sec. 3.4), and training and inference (in Sec. 3.5).

3.1. Task Description

This section first delineates the detailed description of the newly-emerging EgoHOS task. The EgoHOS task includes the segmentation of left- and right-hands, 1st-order interacting objects, and 2nd-order interacting objects. Following the work proposed by Zhang *et al.* [9], we focus on the segmentation of hands and 1st-order interacting objects, *i.e.*, objects that are *directly contacted* by hands. Given an egocentric image $\mathbf{I} \in \mathbb{R}^{H \times W \times 3}$, the goal is to predict the masks of the following entities: hands \mathbf{M}_H , left-hand objects \mathbf{M}_O^L (objects directly interacting with the left hand), right-hand objects \mathbf{M}_O^R (objects directly interacting with the right hand), and two-hand objects \mathbf{M}_O^T (objects interacting with both hands simultaneously).

3.2. Overall Architecture

The Overall diagram of the proposed ORMNet is shown in Fig. 2, which consists of data preparation (left), training (middle), and inference (right). The detailed information about data preparation and inference will be introduced in Section 3.4. The model architecture consists of an encoder, a bottleneck, and a decoder with multiple branches. The encoder is used to extract multi-scale distinguishing features of the input

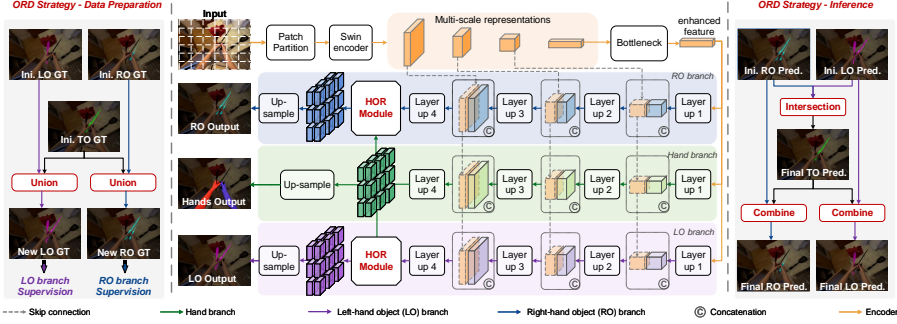


Figure 2: Overall diagram of the proposed end-to-end ORMNet, which incorporates the HOR module and ORD strategy to effectively predict hands, left-hand objects (LO), right-hand objects (RO), and two-hand objects (TO). The ORD strategy consists of data preparation (left), training (middle), and inference (right).

egocentric image, the bottleneck is used to enhance the extracted global features, and different branches of the decoder are used to predict the final segmentation masks for diverse categories.

Specifically, taking an egocentric image \mathbf{I} as input, the first step of ORMNet is to use the image encoder to extract the multi-scale representative features $\mathbf{F} = \{\mathbf{F}_i \in \mathbb{R}^{H_i \times W_i \times C_i} \mid i = 0, 1, \dots, N\}$ by a series of down-samplings with a factor of 2, where H_i , W_i , and C_i are the height, width, and channel of the i^{th} -stage feature map, respectively. The image encoder used in practice is the Swin Transformer encoder [41], and N is set to 3. The extraction process of generating multi-scale features in the encoder can be expressed as follows:

$$\mathbf{F}_{i+1} = f_{enc}^{i+1}(\mathbf{F}_i \mid W_{enc}^{i+1}), \quad i \in \{0, 1, \dots, N-1\}, \quad (1)$$

$$\mathbf{F}_0 = f_{enc}^0(\mathbf{I} \mid W_{enc}^0), \quad (2)$$

where the $f_{enc}^i(\cdot)$ denotes the encoder stage for generating the i^{th} -stage feature map, and the W_{enc}^i represents corresponding parameters.

After generating the multi-scale features, the final global feature map \mathbf{F}_N is sent into the bottleneck to enhance the representation of the encoded feature. Following the work [18], the bottleneck is composed of a patch merging layer and two Swin

Transformer blocks, which are denoted as follows:

$$\mathbf{F}_{ehc} = f_{bot}(\mathbf{F}_N | W_{bot}), \quad (3)$$

where the \mathbf{F}_{ehc} represents the enhanced final feature map, and the $f_{bot}(\cdot)$ denotes the bottleneck network with the parameter of W_{bot} .

Taking the enhanced global feature \mathbf{F}_{ehc} and multi-scale features $\mathbf{F}' = \{\mathbf{F}_i | i = 0, 1, \dots, N-1\}$ as input, different decoder branches are used to predict the final mask of each category. Following the previous work [9], ORMNet also contains the contact boundary (CB) decoder branch to predict the mask of the contact boundary. For simplification, we remove it in Fig. 2 (middle). In each decoder branch, $N+1$ decoder stages are employed to predict the masks. And the output feature of each stage is concatenated with corresponding encoded features by skip-connection [42] as the input to the next stage. The final up-sampling layer is used to recover the resolution to the same as the input egocentric image. The process of each decoder branch can be denoted as:

$$\mathbf{D}_0 = f_{up}^0(\mathbf{F}_{ehc}), \quad (4)$$

$$\mathbf{D}_{i+1} = f_{up}^{i+1}(f_{cat}(\mathbf{D}_i, \mathbf{F}_{N-1-i})), \quad (5)$$

$$\mathbf{M} = f_{us}(\mathbf{D}_N), \quad (6)$$

where the $f_{up}^i(\cdot)$ means the i^{th} decoder stage, which outputs \mathbf{D}_i as decoded feature map. The $f_{cat}(\cdot)$ means the concatenation operation, the $f_{us}(\cdot)$ represents the final up-sampling layer, and the \mathbf{M} denotes the predicted mask of this decoder branch.

3.3. Hand-Object Relation Module

Among the egocentric visual information, the hand information of the HMD wearer is the most prominent and representative because we can easily recognize hands by shape and texture [20]. Moreover, the contacted objects can be accurately identified based on whether they are interacting with hands rather than appearance and texture cues. Therefore, using hand features to enhance the extraction and expression of interacting-object features is beneficial to the EgoHOS task. While certain sequential methods [9] employ predicted hand masks to segment interacting objects, the performance of this coarse approach cannot effectively excavate the relationships between

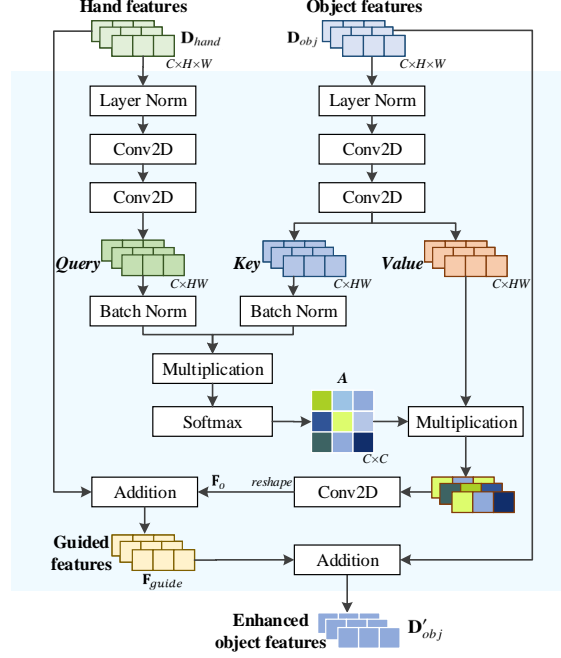


Figure 3: Detailed architecture of the proposed HOR module. Taking the features of hands and interacting objects as input, this module accomplishes hand-guided attention to model the relationship between them, promoting the object feature learning of the network.

them. This paper proposes the HOR module to model the correlation between hand and object features in interaction, which uses representative hand features as priors and guidance and utilizes the hand-guided attention mechanism to guide the learning of interacting-object features, as shown in Fig. 3.

Assume we use separate decoder branches for hands and interacting objects, taking the N^{th} layer of hand features $\mathbf{D}_{hand} \in \mathbb{R}^{\hat{C} \times \hat{H} \times \hat{W}}$ from the hand decoder branch and the object features $\mathbf{D}_{obj} \in \mathbb{R}^{\hat{C} \times \hat{H} \times \hat{W}}$ generated by the object decoder branch as input, this module aims to use hand features to enhance the representation of interacting objects, where \hat{C} , \hat{H} , and \hat{W} are the channel, height, and width of the feature map. First, two stacked convolution operations are used after the LayerNorm layer to generate the query, key, and value. The query $Q \in \mathbb{R}^{\hat{C} \times \hat{H} \times \hat{W}}$ is generated from hand features, and the key $K \in \mathbb{R}^{\hat{C} \times \hat{H} \times \hat{W}}$ and value $V \in \mathbb{R}^{\hat{C} \times \hat{H} \times \hat{W}}$ are generated by interacting-object features,

which can be denoted as follows:

$$Q = f_{conv}(f_{conv}(f_{ln}(\mathbf{D}_{hand}))), \quad (7)$$

$$K, V = f_{conv}(f_{conv}(f_{ln}(\mathbf{D}_{obj}))), \quad (8)$$

where the $f_{conv}(\cdot)$ and $f_{ln}(\cdot)$ represent the convolution and LayerNorm layers. After that, the query, key, and value are used to perform the hand-guided attention operation, *i.e.*:

$$\mathbf{A} = \delta(f_{Matmul}(Norm(Q), Norm(K^T))), \quad (9)$$

$$\mathbf{F}_o = f_{conv}(f_{Matmul}(\mathbf{A}, V)), \quad (10)$$

where the \mathbf{F}_o is the output after convolution, the $f_{Matmul}(x, y)$ means the matrix multiplication between x and y , and the $\delta(\cdot)$ represents the softmax function. Then, the input hand features are added to the \mathbf{F}_o to generate the guided features. Finally, the element-wise addition between guided features and original object features is performed to enhance the representation of the interacting-object features, which can be described as follows:

$$\mathbf{F}_{guide} = \mathbf{F}_o + \mathbf{D}_{hand}, \quad (11)$$

$$\mathbf{D}'_{obj} = \mathbf{D}_{obj} + \mathbf{F}_{guide}, \quad (12)$$

where the \mathbf{D}'_{obj} is the final enhanced interacting-object features. In this way, the relationships between hands and interacting objects are established explicitly by the hand-guided attention mechanism. Therefore, hand features can be used as queries to extract more representative and distinguishing object features, improving the interacting-object segmentation performance.

3.4. Object Relation Decoupling Strategy

Based on the proposed HOR module, a naive way is to use one decoder branch to predict hands and another decoder branch to predict interacting objects. Then, the HOR module can establish the relation between hands and interacting objects, as shown in Sec. 3.3. However, this paper argues that in this way, the three different types of

interacting objects, *i.e.*, left-hand objects, right-hand objects, and two-hand objects, are coupled.

To be specific, we observe that the two-hand object interacts with both left and right hands, so it encompasses attributes of both the left-hand and right-hand objects. Based on this observation, we contend that two-hand objects can be conceptualized as the *intersection* of the remaining two categories (left-hand object and right-hand object). Therefore, if we remove the two-hand object category during training and represent this category by using the other two categories in inference, the network can be relieved from classifying “whether the object is interacting with both hands at the same time” and focus only on the left- and right-interaction.

Therefore, different from previous work, our method proposes the ORD strategy to decouple the three kinds of interacting objects according to observed relations. In practice, the ORD process can be divided into data preparation, training, and inference. During data preparation, since two-hand objects encompass attributes of left-hand and right-hand objects, the ground truth (GT) of the two-hand object is treated as the left-hand and right-hand objects to generate new object labels. Specifically, as shown in Fig. 2 (left), the new GT of the left/right-hand object is obtained by the *union* operation between the original left/right-hand object and two-hand object labels. The process is shown below:

$$\mathbf{G}'_{lo} = \mathbf{G}_{lo} \cup \mathbf{G}_{to} = \{(x \in \mathbf{G}_{lo}) \vee (x \in \mathbf{G}_{to})\}, \quad (13)$$

$$\mathbf{G}'_{ro} = \mathbf{G}_{ro} \cup \mathbf{G}_{to} = \{(x \in \mathbf{G}_{ro}) \vee (x \in \mathbf{G}_{to})\}, \quad (14)$$

where the \cup means the union operation, the \mathbf{G}_{lo} , \mathbf{G}_{ro} , and \mathbf{G}_{to} are the original labels for left-hand objects, right-hand objects, and two-hand objects, respectively. The \mathbf{G}'_{lo} and \mathbf{G}'_{ro} represent the generated new supervision signals for left-hand objects and right-hand objects.

Then, during training, we use separate decoder branches to predict the left-hand objects and right-hand objects, as shown in Fig. 2 (middle). The left-hand object decoder output \mathbf{M}_{lo} can be obtained by up-sampling the outcome \mathbf{D}'_{lo} of the HOR module from equation 12, and the right-hand object decoder output \mathbf{M}_{ro} can be obtained by up-sampling the outcome \mathbf{D}'_{ro} of the HOR module from equation 12. \mathbf{G}'_{lo} and \mathbf{G}'_{ro} are

utilized to supervise these two branches, which can be expressed as follows,

$$\mathcal{L}_{lo} = l_{ce}(\mathbf{M}_{lo}, \mathbf{G}'_{lo}), \quad (15)$$

$$\mathcal{L}_{ro} = l_{ce}(\mathbf{M}_{ro}, \mathbf{G}'_{ro}), \quad (16)$$

where the \mathcal{L}_{lo} and \mathcal{L}_{ro} denote the loss of left-hand objects and right-hand objects, which we use the cross entropy $l_{ce}(\cdot)$ in practice.

In inference, after obtaining the decoder output of left- and right-hand objects \mathbf{M}_{lo} and \mathbf{M}_{ro} , the results of two-hand objects are generated by an ingenious operation, *i.e.*, **intersection**. The final predictions of the left-hand objects and the right-hand objects have to remove the region of the two-hand objects, as shown in Fig. 2 (right) and follows,

$$\mathbf{M}_O^T = \mathbf{M}_{lo} \cap \mathbf{M}_{ro} = \{(x \in \mathbf{M}_{lo}) \wedge (x \in \mathbf{M}_{ro})\}, \quad (17)$$

$$\mathbf{M}_O^L = \mathbf{M}_{lo} - \mathbf{M}_O^T = \{(x \in \mathbf{M}_{lo}) \wedge (x \notin \mathbf{M}_O^T)\}, \quad (18)$$

$$\mathbf{M}_O^R = \mathbf{M}_{ro} - \mathbf{M}_O^T = \{(x \in \mathbf{M}_{ro}) \wedge (x \notin \mathbf{M}_O^T)\}, \quad (19)$$

where the \cap means the intersection operation. The \mathbf{M}_O^L , \mathbf{M}_O^R , and \mathbf{M}_O^T are the final left-, right-, and two-hand object predictions, respectively.

The innovative ORD strategy decouples the two-hand objects during training using pure mathematical intersection and union operations. This approach enables the algorithm to prioritize the interaction between hands and objects, thereby diminishing the emphasis on classification and decreasing the confusion and ambiguity of the algorithm.

3.5. Training and Inference

The overall ORMNet is trained by the weighted cross-entropy loss function between predictions and GTs of hands, left-hand objects, right-hand objects, and contact boundaries [9]. The overall loss function \mathcal{L} can be computed by:

$$\begin{aligned} \mathcal{L} = & \alpha(l_{ce}(\mathbf{M}_{lo}, \mathbf{G}'_{lo}) + l_{ce}(\mathbf{M}_{ro}, \mathbf{G}'_{ro})) + \\ & \gamma l_{ce}(\mathbf{M}_H, \mathbf{G}_h) + \lambda l_{ce}(\mathbf{M}_{CB}, \mathbf{G}_{cb}), \end{aligned} \quad (20)$$

Algorithm 1 ORMNet

ORD STRATEGY - DATA PREPARATION

$$\mathbf{G}'_{lo} = \mathbf{G}_{lo} \cup \mathbf{G}_{to}$$

$$\mathbf{G}'_{ro} = \mathbf{G}_{ro} \cup \mathbf{G}_{to}$$

TRAIN

Initialize: $W = \{W_{enc}, W_{dec}^h, W_{dec}^{lo}, W_{dec}^{ro}, W_{dec}^{cb}\}, \alpha, \beta, \gamma, \lambda$

Prediction: $\mathbf{M}_{lo}, \mathbf{M}_{ro}, \mathbf{M}_H, \mathbf{M}_{CB}$

Loss: $\mathcal{L} = \alpha(l_{ce}(\mathbf{M}_{lo}, \mathbf{G}'_{lo}) + l_{ce}(\mathbf{M}_{ro}, \mathbf{G}'_{ro})) + \gamma l_{ce}(\mathbf{M}_H, \mathbf{G}_h) + \lambda l_{ce}(\mathbf{M}_{CB}, \mathbf{G}_{cb})$

Back Propagation: $W \leftarrow W - \beta \nabla \mathcal{L}(W)$

Return: W

INFERENCE

Prediction: $\mathbf{M}_{lo}, \mathbf{M}_{ro}, \mathbf{M}_H, \mathbf{M}_{CB}$

ORD Strategy - Inference: $\mathbf{M}_O^T = \mathbf{M}_{lo} \cap \mathbf{M}_{ro}$

$$\mathbf{M}_O^L = \mathbf{M}_{lo} - \mathbf{M}_O^T$$

$$\mathbf{M}_O^R = \mathbf{M}_{ro} - \mathbf{M}_O^T$$

Return: $\mathbf{M}_H, \mathbf{M}_{CB}, \mathbf{M}_O^T, \mathbf{M}_O^L, \mathbf{M}_O^R$

where α , γ , and λ denote the loss weight of interacting objects, hands, and contact boundaries [9], respectively. \mathbf{M}_{CB} presents the output of the contact boundary decoder branch, which is supervised by \mathbf{G}_{cb} . Following previous work [9], the GT of the contact boundary is generated by the overlapping region of the dilated hand and interacting-object masks. \mathbf{M}_H denotes the output of the hand decoder branch, which is supervised by \mathbf{G}_h .

For inference, as stated in Sec. 3.4, the decoder branches predict the masks of hands, left-hand objects, and right-hand objects. Then, the final predicted masks of left-hand objects, right-hand objects, and two-hand objects can be obtained by the proposed ORD strategy. The overall diagram for training and inference is shown in Algorithm 1.

4. Experiments

4.1. Datasets and Metrics

To validate the effectiveness of the proposed ORMNet, we compare its performance with different methods on the EgoHOS [9] in-domain test set. Additionally, we employed the EgoHOS out-of-domain test set as well as a dataset we developed from the HOI4D [43] dataset, referred to as mini-HOI4D, to assess the generalization capability of our ORMNet.

EgoHOS. The EgoHOS [9] dataset consists of 11,743 egocentric images containing per-pixel segmentation labels of hands and interacting objects gathered from Ego4D [24], EPICKITCHEN [26], THU-READ [44], and their own collected egocentric videos. Among them, 8,993 images are used for training, 1,124 images are for validation, 1,126 images are used for in-domain testing, and 500 images are used for out-of-domain testing.

mini-HOI4D. Since the EgoHOS task is an emerging problem, to the best of our knowledge, no suitable datasets other than the EgoHOS dataset can be used to validate the generalization of the model. As a result, we selected the relatively similar HOI4D [43] dataset and further processed and aligned its annotations to ensure its applicability for the EgoHOS task requirements. Ultimately, we generated a new dataset, named mini-HOI4D, comprising 1,095 egocentric images with corresponding hands and interacting object annotations, which can be used to assess and compare the generalization capabilities of our ORMNet and other approaches.

This paper uses the most common and widely used metrics in the segmentation task to evaluate the performance, *i.e.*, Intersection-over-Union (IoU) and pixel Accuracy (Acc) for each category. Mean IoU (mIoU) and mean accuracy (mAcc) are also employed to indicate the overall performance.

4.2. Implementation Details

The experiments were conducted on 4 NVIDIA RTX 6000 Ada GPUs. The batch size was set to 12. Data preparation included cropping the image to (448, 448) and normalization with the mean of [106.011, 95.400, 87.429], and the standard variation

was set to [64.357, 60.889, 61.419]. Following previous work [9], we also used the Swin Transformer as the backbone. The patch size was set to 4, and the window size was set to 12. The AdamW optimizer was used in the experiment, the learning rate was set to 1e-5, and the weight decay was set to 0.01. The learning rate was set dynamically, *i.e.*, from 0 to 10,000 iterations, the learning rate increased linearly to 1e-4, and from 10,000 iterations to the maximum iteration, the learning rate decreased linearly to 0. The maximum number of iterations in the experiment was set to 180,000.

4.3. Quantitative Results

4.3.1. In-domain Results

Table 1: Comparison results on the EgoHOS in-domain test set measured by IoU/Acc and mIoU/mAcc. The blue letters represent the best results. The “ \mathcal{r} ” means the method with data augmentation, the “ \diamond ” means the method introduced contact boundary, and the “ \mathcal{b} ” means the method with data augmentation and contact boundary.

Method	Type	Backbone	Left hand	Right hand	Left-hand objects	Right-hand objects	Two-hand objects	Overall
			IoU(%) Acc(%)	IoU(%) Acc(%)	IoU(%) Acc(%)	IoU(%) Acc(%)	IoU(%) Acc(%)	mIoU(%) mAcc(%)
Segformer[16]	parallel	MiT[16]	62.49 75.47	64.77 78.13	4.03 4.57	3.01 3.17	5.13 5.57	27.89 33.38
SCTNet[45]	parallel	SCTNet[45]	81.94 90.25	82.12 89.92	17.77 24.49	16.60 20.79	21.74 29.08	44.03 50.91
Para. ¹ [9]	parallel	Swin-B	77.57 -	81.06 -	54.83 -	38.48 -	39.14 -	58.22 -
Segformer[16]	parallel	Swin-B	65.36 78.20	66.26 79.21	11.63 15.45	8.07 9.24	12.48 15.97	32.76 39.61
Para.[9]	parallel	Swin-B	69.08 75.57	73.50 75.93	48.67 39.50	36.21 39.33	37.46 42.58	52.98 54.58
Segmenter[46]	parallel	Swin-B	82.20 89.87	83.28 91.92	46.22 62.69	34.79 45.59	51.10 62.78	59.52 70.57
UperNet[19]	parallel	Swin-B	89.88 89.86	91.39 91.32	36.22 37.24	40.55 42.26	45.54 49.27	60.71 61.99
Segmenter[46]	parallel	ViT[47]	88.47 95.66	89.29 95.08	49.87 61.14	40.60 57.07	46.96 60.81	63.04 73.95
MaskFormer[48]	parallel	Swin-B	90.45 95.90	91.95 96.41	43.51 67.08	41.04 52.91	54.65 64.86	64.32 75.43
Mask2Former[49]	parallel	Swin-B	90.74 96.01	92.25 96.20	44.22 53.97	46.05 58.10	51.13 60.48	64.88 72.95
Seq.[9]	sequential	Swin-B	73.17 -	80.56 -	54.83 -	38.48 -	39.14 -	57.24 -
Seq. ² [9]	sequential	Swin-B	77.25 -	81.17 -	59.05 -	40.85 -	49.94 -	61.65 -
Seq. ³ [9]	sequential	Swin-B	87.70 -	88.79 -	58.32 -	40.18 -	46.24 -	64.25 -
Seq. ⁴ [9]	sequential	Swin-B	87.70 95.77	88.79 91.29	62.20 66.67	44.40 59.85	52.77 62.21	67.17 75.16
ORMNet	parallel	Swin-B	92.34 96.64	93.64 96.81	60.07 71.79	56.69 68.71	54.73 65.85	71.49 79.96

Comparison results on EgoHOS in-domain test set. To validate the effectiveness of the proposed ORMNet, we conducted experiments by training on the EgoHOS train set

and testing on the EgoHOS in-domain test set. Due to the novelty of the EgoHOS task, we selected a set of novel state-of-the-art general segmentation algorithms [16, 46, 48, 49, 45] as compared parallel methods. Furthermore, we ensured a comprehensive comparison by incorporating all existing methods [9] tailored for the EgoHOS task in this evaluation. The results are presented in Table 1. In general, the proposed ORMNet far outperforms all previous methods in most categories on both metrics. Specifically, compared with the previous best parallel method - Mask2Former [49], our method has demonstrated pronounced advancements across various categories and exhibited particularly notable enhancements in interacting-object segmentation. For example, our method showcases substantial enhancements of 15.85%, 10.64%, and 3.6% on left-, right-, and two-hand objects, respectively. Moreover, compared with the results of the previous best sequential methods Seq^b, our ORMNet improves IoU by more than 4% on both the left and right hands. The most substantial enhancement is observed in the right-hand objects, surpassing 12%. Finally, compared with the previous best method, our proposed method attains a commendable advancement of 4.33% and 4.55% in mIoU and mAcc, respectively. These results profoundly demonstrate the state-of-the-art segmentation performance achieved by the proposed ORMNet on the basis of end-to-end optimization, leveraging the HOR module and the ORD strategy to model the correlations between hands and objects as well as objects and objects.

Table 2: Comparison results on the EgoHOS out-of-domain test set. The blue letters represent the best results. The “b” means the method with data augmentation and contact boundary.

Method	Type	Backbone	Left hand	Right hand	Left-hand objects	Right-hand objects	Two-hand objects	Overall
			IoU(%) Acc(%)	IoU(%) Acc(%)	IoU(%) Acc(%)	IoU(%) Acc(%)	IoU(%) Acc(%)	mIoU(%) mAcc(%)
Segformer[16]	parallel	MiT[16]	71.97 87.33	71.44 81.75	7.60 8.34	5.00 5.65	4.91 5.95	32.18 37.80
Segformer[16]	parallel	Swin-B	74.01 86.80	70.84 79.44	15.61 21.77	7.32 9.56	8.29 11.67	35.21 41.85
SCTNet[45]	parallel	SCTNet[45]	87.12 94.62	86.29 90.92	31.18 49.14	19.70 27.47	13.32 17.12	47.52 55.85
UperNet[19]	parallel	Swin-B	93.17 96.89	93.96 96.00	42.53 64.83	28.88 54.59	24.35 27.83	56.58 68.03
Segmenter[46]	parallel	Swin-B	83.13 91.22	84.85 92.56	57.97 72.44	38.59 52.75	44.98 52.88	61.90 72.37
Maskformer[48]	parallel	Swin-B	92.69 95.58	94.02 96.10	51.81 70.53	39.84 60.49	39.43 46.52	63.56 73.84
Mask2former[49]	parallel	Swin-B	91.46 97.05	93.04 96.38	53.41 64.39	44.90 64.18	35.61 39.78	63.68 72.36
Segmenter[46]	parallel	ViT[47]	89.40 95.02	90.58 94.86	52.73 75.75	43.88 56.34	42.33 51.08	63.78 74.61
Seq. ^b [9]	sequential	Swin-B	81.77 87.83	78.82 85.98	46.93 57.17	26.40 43.85	42.38 54.76	55.26 65.92
ORMNet	parallel	Swin-B	94.47 97.09	94.41 96.69	51.56 72.30	36.80 60.90	41.84 46.28	63.82 74.65

4.3.2. Out-of-domain Results

1) *Comparison results on EgoHOS out-of-domain test set.* In order to test the generalization performance of different models, the EgoHOS dataset provides 500 out-of-domain images, which are captured from YouTube and annotated manually. Thus, We compare ORMNet with different parallel and sequential models by directly testing saved best models on the EgoHOS out-of-domain test set, results are shown in Table 2. It can be observed that the results of our proposed ORMNet on the two metrics of most categories have obtained significant generalization performance. Among them, the IoU of the left and right hand exceed 94%, and the Acc. of these two categories exceed 96%. The segmentation results on various interacting-object categories also achieve balanced performance. Finally, our ORMNet achieves state-of-the-art generalization performance in overall mIoU and mAcc metrics on the EgoHOS out-of-domain test set.

Table 3: Comparison results on the mini-HOI4D test set. The blue letters represent the best results. The “b” means the method with data augmentation and contact boundary.

Method	Type	Backbone	Left hand	Right hand	Right-hand objects	Two-hand objects	Overall
			IoU(%) Acc(%)	IoU(%) Acc(%)	IoU(%) Acc(%)	IoU(%) Acc(%)	mIoU(%) mAcc(%)
Segformer[16]	parallel	Swin-B	27.73 87.97	53.27 66.91	8.43 9.72	9.30 13.40	24.68 44.50
Segformer[16]	parallel	MiT[16]	30.16 92.13	56.44 72.42	5.17 5.52	12.02 13.41	25.95 45.87
SCTNet[45]	parallel	SCTNet[45]	35.83 95.25	66.29 71.27	17.72 22.68	20.98 29.98	35.21 54.80
Segmenter[46]	parallel	Swin-B	70.31 89.02	73.78 89.23	21.82 43.75	44.98 56.97	52.72 69.74
UperNet[19]	parallel	Swin-B	54.82 97.71	84.43 86.04	20.34 25.77	29.34 36.58	47.23 61.53
MaskFormer[48]	parallel	Swin-B	58.50 96.63	83.66 87.83	35.28 44.81	56.91 73.47	58.59 75.69
Segmenter[46]	parallel	ViT[47]	74.70 94.03	85.58 92.34	22.38 44.42	58.67 73.99	60.33 76.20
Mask2Former[49]	parallel	Swin-B	70.13 97.48	88.57 89.38	32.37 45.22	55.72 74.17	61.70 76.56
Seq. ^b [9]	sequential	Swin-B	8.74 40.90	34.60 38.05	23.88 28.99	53.96 61.67	30.30 42.40
ORMNet	parallel	Swin-B	70.39 97.79	89.76 93.09	27.56 49.35	60.08 68.01	61.95 77.06

2) *Comparison results on mini-HOI4D dataset.* In order to comprehensively validate the generalizability of the proposed method, we also assess the generalization capabilities of algorithms using a completely different mini-HOI4D dataset. It should

Table 4: Ablation results on the EgoHOS in-domain test set under the same setting measured by IoU and mIoU. Lh: left hand, rh: right hand, lo: left-hand object, ro: right-hand object, to: two-hand object.

Method	Lh (%)	Rh (%)	Lo (%)	Ro (%)	To (%)	mIoU (%)
Basic	90.47	91.02	44.11	45.57	51.08	64.45
Basic+ORD	93.14	93.73	60.86	54.58	49.69	70.40
Basic+HOR	92.76	93.36	44.15	53.68	51.85	67.16
Basic+ORD+HOR	92.34	93.64	60.07	56.69	54.73	71.49

be noted that since the original HOI4D [43] dataset contains very few samples of left-hand objects, we do not perform testing on left-hand object category. We also utilized the saved best models to test on the mini-HOI4D dataset without further training procedures, the comparison results are shown in Table 3. Overall, our proposed ORMNet outperforms all the previous parallel and sequential methods concerning mIoU and mAcc. Our method excels notably in hand segmentation, *i.e.*, 1.57% and 3.71% improvements on IoU and Acc for the right hand compared with the previous best Mask2Former model. Our method also competes well in interacting-object segmentation, yielding commendable outcomes. Therefore, it can be deduced from the results of the EgoHOS out-of-domain and mini-HOI4D test sets that our proposed ORMNet exhibits superior generalization capabilities in contrast to the comparative methods.

4.3.3. Ablation Study

In order to verify the effectiveness of the proposed method alongside its corresponding sub-module and strategy, we conduct the ablation study in this section. The experimental results are shown in Table 4. The basic model uses Swin-B as the encoder and uses three decoder branches to predict hands, contact boundaries, and interacting objects. This basic model is a naive solution for the EgoHOS task and does not model any relationships between hands and interacting objects, so its results are relatively poor. The 2nd and 3rd rows of the table show the results after adding the ORD strategy and HOR module independently, which proves that adding them to the basic model is beneficial. The last row is the result after integrating the ORD strategy and the HOR module. By explicitly modeling the relations between *hands and objects* as well as *objects and objects*, the segmentation accuracy achieves its peak performance. Generally

Table 5: The experimental results using different hyper-parameters. α , γ , and λ are the weights of interacting objects, hands, and CB losses.

α	γ	λ	Lh (%)	Rh (%)	Lo (%)	Ro (%)	To (%)	mIoU (%)
1.0	1.0	1.0	90.66	91.80	57.38	56.20	52.12	69.63
1.0	0.5	0.5	89.74	90.56	57.8	55.46	51.08	68.93
0.5	0.5	1.0	90.22	91.10	57.78	55.59	50.81	69.10
0.5	1.0	0.5	92.34	93.64	60.07	56.69	54.73	71.49

speaking, although the effect improvement brought by the ORD strategy is higher than that of the HOR module, using these two modules and strategies simultaneously can further improve the segmentation performance, which verifies the effectiveness of our proposed method and sub-methods.

4.3.4. Hyper-parameter Study

The method presented in this paper requires setting multiple hyper-parameters for total training loss, *i.e.*, α , γ , and λ . This section conducts experiments on the configurations of different hyper-parameters, results are shown in Table 5. We assign the values of α , γ , and λ based on the relative significance of the interacting objects, hands, and contact boundaries. In the 1st row, all categories are considered equal importance, while in subsequent experiments (*i.e.*, 2nd, 3rd and 4th), we regard the interacting objects, CBs, and hands as the most crucial, respectively. The results lead to the inference that amplifying the importance of hands can yield enhancements in the method’s performance, which can be explained intuitively because the proposed HOR module leverages hands as prior knowledge for interacting-object feature enhancement.

4.4. Qualitative Results

4.4.1. In-domain Results

Results on EgoHOS in-domain test set. This section shows the visualization results on the EgoHOS in-domain test set compared with the previous best sequential method Seq.^b, as shown in Fig. 4. We can observe that our method has better performance in segmenting hands, as shown in the results of the 1st and 2nd rows. Moreover, since our method proposes an ORD strategy to model the relationship between diverse interacting objects, ORMNet also has better consistency and accuracy when segmenting

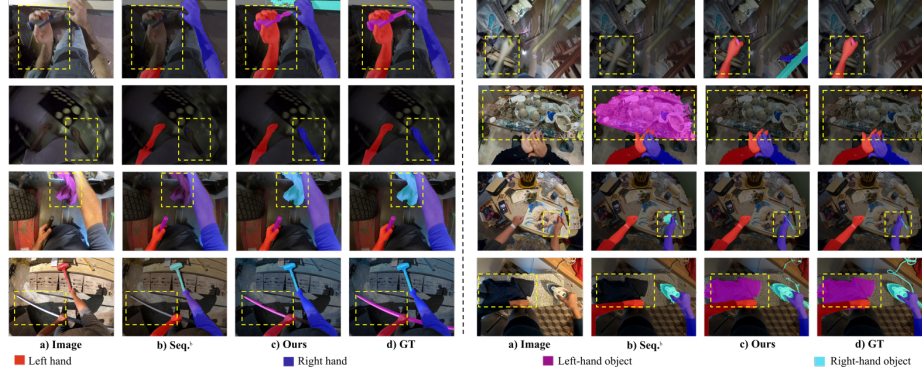


Figure 4: Visualization results of the ORMNet compared with the sequential method Seq.^b [9] on the EgoHOS in-domain test set. The main improvements are highlighted in the dashed yellow box.

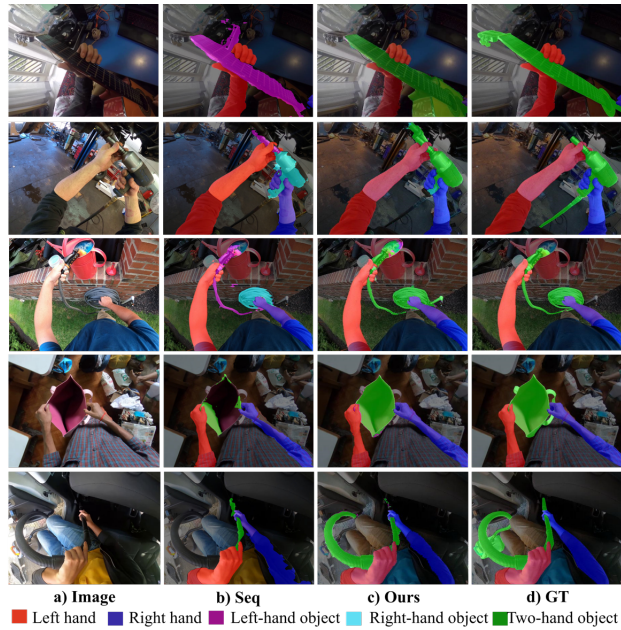


Figure 5: Visualization results of **two-hand objects** on the EgoHOS in-domain test set compared with sequential method Seq.^b [9].

objects, as shown in the results of the 3rd and 4th rows. Furthermore, although our method does not predict two-hand objects through the learnable network, the performance is also more significant than the compared method, which is shown in Fig. 5.

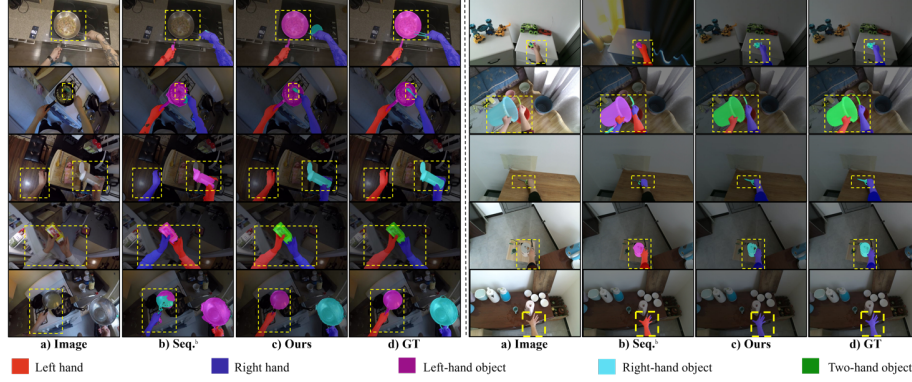


Figure 6: Visualization results of the ORMNet compared with the sequential method [9] on the EgoHOS out-of-domain test set (left) and mini-HOI4D dataset (right). The main improvements are highlighted in the dashed yellow box.

In the results of the comparative method, the two-hand objects or part of them may be segmented into left- and right-hand objects. However, our method only focuses on the objects that the hands interact with during the learning process using the ORD strategy rather than concentrating on “whether the object interacts with the left and right hands at the same time,” thereby enhancing the segmentation consistency and accuracy of two-hand objects.

4.4.2. Out-of-domain Results

1) *Results on EgoHOS out-of-domain test set.* We visualize the comparative results on the EgoHOS out-of-domain test set with the Seq^b method in Fig. 6 (left). The figure shows that our ORMNet has stronger generalization than the compared sequential model. Specifically, our method can segment and identify left and right hands accurately, as shown in the 3rd to the last rows of results. Furthermore, our method can precisely segment and recognize different kinds of interacting objects, as shown in the first and second rows in the figure.

2) *Results on mini-HOI4D dataset.* We visualize the comparative results on the mini-HOI4D test set with the Seq^b method in Fig. 6 (right). It can be observed that the contrasting sequential method easily confuses the left and right hands, such as 1st, 2nd, 4th, and 5th rows of the results. In contrast, our method exhibits robust generalization

capabilities coupled with outstanding segmentation performance.

5. Conclusion

This paper introduces the ORMNet to effectively handle the EgoHOS task while achieving end-to-end optimization by incorporating two parts. First, the HOR module is proposed to facilitate the modeling of hand-object interactions through hand-guided cross-attention, enhancing the network’s adaptability to learn comprehensive interacting-object representations. Second, this paper designs an ingenious ORD strategy to decouple the two-hand objects, thereby reducing the confusion of the network about interacting-object classification and emphasizing the left/right interactions.

However, there remains a limitation that needs to be addressed. Specifically, the EgoHOS task focuses solely on predicting hands (left- and right-hand) and interacting objects (left-hand object, right-hand object, and two-hand object) without inferring the object’s name or semantic information. Consequently, this limits the comprehensive description of people’s actions. To address this issue, we plan to enhance and refine the EgoHOS task in future work. Our goal is to incorporate the prediction of interacting-object semantic information alongside hand-object segmentation, thereby expanding the practical applicability of the algorithm in real-world scenarios.

6. Acknowledgements

The research work was conducted in the JC STEM Lab of Machine Learning and Computer Vision funded by The Hong Kong Jockey Club Charities Trust.

References

- [1] W. Ouyang, Z. Xu, J. Xu, Q. Wang, Y. Xu, Mixingmask: A contour-aware approach for joint object detection and instance segmentation, *Pattern Recognition* 155 (2024) 110620.
- [2] A. Dhamanaskar, M. Dimiccoli, E. Corona, A. Pumarola, F. Moreno-Noguer, Enhancing egocentric 3d pose estimation with third person views, *Pattern Recognit.* 138 (2023) 109358.

- [3] P. Xue, S. Niu, A novel active contour model based on features for image segmentation, *Pattern Recognit.* 155 (2024) 110673.
- [4] E. Santos, V. Castillo, Apple vision pro: Comments in healthcare, *arXiv preprint arXiv:2401.08685* (2024).
- [5] Y. Zhang, X. Hu, K. Kiyokawa, X. Yang, Add-on occlusion: Building an occlusion-capable optical see-through head-mounted display with hololens 1, in: *IEEE Conference on Virtual Reality and 3D User Interfaces Abstracts and Workshops (VRW)*, IEEE, 2023, pp. 1003–1004.
- [6] T. Suveges, S. McKenna, Unsupervised mapping and semantic user localisation from first-person monocular video, *Pattern Recognition* (2024) 110923.
- [7] M. M. Alam, M. T. Islam, S. M. Rahman, Unified learning approach for egocentric hand gesture recognition and fingertip detection, *Pattern recognition* 121 (2022) 108200.
- [8] H. Qi, H. Zhou, J. Dong, X. Dong, Small sample image segmentation by coupling convolutions and transformers, *IEEE Transactions on Circuits and Systems for Video Technology* (2023).
- [9] L. Zhang, S. Zhou, S. Stent, J. Shi, Fine-grained egocentric hand-object segmentation: Dataset, model, and applications, in: *European Conference on Computer Vision*, Springer, 2022, pp. 127–145.
- [10] Y. Lin, Y. Lan, S. Wang, A method for evaluating the learning concentration in head-mounted virtual reality interaction, *Virtual Reality* 27 (2) (2023) 863–885.
- [11] R. Shi, Y. Wei, X. Qin, P. Hui, H.-N. Liang, Exploring gaze-assisted and hand-based region selection in augmented reality, *Proceedings of the ACM on Human-Computer Interaction* 7 (ETRA) (2023) 1–19.
- [12] C. Li, C. Wong, S. Zhang, N. Usuyama, H. Liu, J. Yang, T. Naumann, H. Poon, J. Gao, Llava-med: Training a large language-and-vision assistant for

biomedicine in one day, *Advances in Neural Information Processing Systems* 36 (2024).

- [13] R. Azad, R. Arimond, E. K. Aghdam, A. Kazerouni, D. Merhof, Dae-former: Dual attention-guided efficient transformer for medical image segmentation, in: *International Workshop on PRedictive Intelligence In MEdicine*, Springer, 2023, pp. 83–95.
- [14] Y. Huang, G. Chen, J. Xu, M. Zhang, L. Yang, B. Pei, H. Zhang, L. Dong, Y. Wang, L. Wang, et al., Egoexolearn: A dataset for bridging asynchronous ego- and exo-centric view of procedural activities in real world, in: *Proceedings of the IEEE/CVF Conference on Computer Vision and Pattern Recognition*, 2024, pp. 22072–22086.
- [15] K. Grauman, A. Westbury, L. Torresani, K. Kitani, J. Malik, T. Afouras, K. Ashutosh, V. Baiyya, S. Bansal, B. Boote, et al., Ego-exo4d: Understanding skilled human activity from first-and third-person perspectives, in: *Proceedings of the IEEE/CVF Conference on Computer Vision and Pattern Recognition*, 2024, pp. 19383–19400.
- [16] E. Xie, W. Wang, Z. Yu, A. Anandkumar, J. M. Alvarez, P. Luo, Segformer: Simple and efficient design for semantic segmentation with transformers, *Advances in neural information processing systems* 34 (2021) 12077–12090.
- [17] J. Jain, J. Li, M. T. Chiu, A. Hassani, N. Orlov, H. Shi, Oneformer: One transformer to rule universal image segmentation, in: *Proceedings of the IEEE/CVF Conference on Computer Vision and Pattern Recognition*, 2023, pp. 2989–2998.
- [18] H. Cao, Y. Wang, J. Chen, D. Jiang, X. Zhang, Q. Tian, M. Wang, Swin-unet: Unet-like pure transformer for medical image segmentation, in: *European conference on computer vision*, Springer, 2022, pp. 205–218.
- [19] T. Xiao, Y. Liu, B. Zhou, Y. Jiang, J. Sun, Unified perceptual parsing for scene understanding, in: *Proceedings of the European conference on computer vision (ECCV)*, 2018, pp. 418–434.

- [20] C. Zhang, A. Gupta, A. Zisserman, Helping hands: An object-aware ego-centric video recognition model, in: *Proceedings of the IEEE/CVF International Conference on Computer Vision*, 2023, pp. 13901–13912.
- [21] O. Ronneberger, P. Fischer, T. Brox, U-net: Convolutional networks for biomedical image segmentation, in: *Medical image computing and computer-assisted intervention*, Springer, 2015, pp. 234–241.
- [22] J. Long, E. Shelhamer, T. Darrell, Fully convolutional networks for semantic segmentation, in: *Proceedings of the IEEE conference on computer vision and pattern recognition*, 2015, pp. 3431–3440.
- [23] D. Chatterjee, F. Sener, S. Ma, A. Yao, Opening the vocabulary of egocentric actions, *Advances in Neural Information Processing Systems* 36 (2024).
- [24] K. Grauman, A. Westbury, E. Byrne, Z. Chavis, A. Furnari, R. Girdhar, J. Hamburger, H. Jiang, M. Liu, X. Liu, et al., Ego4d: Around the world in 3,000 hours of egocentric video, in: *Proceedings of the IEEE/CVF Conference on Computer Vision and Pattern Recognition*, 2022, pp. 18995–19012.
- [25] K. Mangalam, R. Akshulakov, J. Malik, Egoschema: A diagnostic benchmark for very long-form video language understanding, *Advances in Neural Information Processing Systems* 36 (2024).
- [26] D. Damen, H. Doughty, G. M. Farinella, S. Fidler, A. Furnari, E. Kazakos, D. Moltisanti, J. Munro, T. Perrett, W. Price, et al., Scaling egocentric vision: The epic-kitchens dataset, in: *Proceedings of the European conference on computer vision (ECCV)*, 2018, pp. 720–736.
- [27] R. Goyal, S. Ebrahimi Kahou, V. Michalski, J. Materzynska, S. Westphal, H. Kim, V. Haenel, I. Fruend, P. Yianilos, M. Mueller-Freitag, et al., The” something something” video database for learning and evaluating visual common sense, in: *Proceedings of the IEEE international conference on computer vision*, 2017, pp. 5842–5850.

- [28] G. A. Sigurdsson, A. Gupta, C. Schmid, A. Farhadi, K. Alahari, Charades-ego: A large-scale dataset of paired third and first person videos, arXiv preprint arXiv:1804.09626 (2018).
- [29] Y. Xu, Y.-L. Li, Z. Huang, M. X. Liu, C. Lu, Y.-W. Tai, C.-K. Tang, Egopca: A new framework for egocentric hand-object interaction understanding, in: Proceedings of the IEEE/CVF International Conference on Computer Vision, 2023, pp. 5273–5284.
- [30] Y. Huang, M. Cai, Z. Li, Y. Sato, Predicting gaze in egocentric video by learning task-dependent attention transition, in: Proceedings of the European conference on computer vision (ECCV), 2018, pp. 754–769.
- [31] Y. Li, M. Liu, J. M. Rehg, In the eye of beholder: Joint learning of gaze and actions in first person video, in: Proceedings of the European conference on computer vision (ECCV), 2018, pp. 619–635.
- [32] K. Q. Lin, J. Wang, M. Soldan, M. Wray, R. Yan, E. Z. Xu, D. Gao, R.-C. Tu, W. Zhao, W. Kong, et al., Egocentric video-language pretraining, Advances in Neural Information Processing Systems 35 (2022) 7575–7586.
- [33] S. Pramanick, Y. Song, S. Nag, K. Q. Lin, H. Shah, M. Z. Shou, R. Chellappa, P. Zhang, Egovlpv2: Egocentric video-language pre-training with fusion in the backbone, in: Proceedings of the IEEE/CVF International Conference on Computer Vision, 2023, pp. 5285–5297.
- [34] H. Wang, M. K. Singh, L. Torresani, Ego-only: Egocentric action detection without exocentric transferring, in: Proceedings of the IEEE/CVF International Conference on Computer Vision, 2023, pp. 5250–5261.
- [35] Y. Li, T. Nagarajan, B. Xiong, K. Grauman, Ego-exo: Transferring visual representations from third-person to first-person videos, in: Proceedings of the IEEE/CVF Conference on Computer Vision and Pattern Recognition, 2021, pp. 6943–6953.

- [36] B. Xu, S. Zheng, Q. Jin, Pov: Prompt-oriented view-agnostic learning for egocentric hand-object interaction in the multi-view world, in: Proceedings of the ACM International Conference on Multimedia, 2023, pp. 2807–2816.
- [37] T. Shiota, M. Takagi, K. Kumagai, H. Seshimo, Y. Aono, Egocentric action recognition by capturing hand-object contact and object state, in: Proceedings of the IEEE/CVF Winter Conference on Applications of Computer Vision, 2024, pp. 6541–6551.
- [38] K. Lee, A. Shrivastava, H. Kacorri, Leveraging hand-object interactions in assistive egocentric vision, *IEEE Transactions on Pattern Analysis and Machine Intelligence* 45 (6) (2023) 6820–6831.
- [39] S. Liu, S. Tripathi, S. Majumdar, X. Wang, Joint hand motion and interaction hotspots prediction from egocentric videos, in: Proceedings of the IEEE/CVF Conference on Computer Vision and Pattern Recognition, 2022, pp. 3282–3292.
- [40] A. Kirillov, E. Mintun, N. Ravi, H. Mao, C. Rolland, L. Gustafson, T. Xiao, S. Whitehead, A. C. Berg, W.-Y. Lo, et al., Segment anything, in: Proceedings of the IEEE/CVF International Conference on Computer Vision, 2023, pp. 4015–4026.
- [41] Z. Liu, Y. Lin, Y. Cao, H. Hu, Y. Wei, Z. Zhang, S. Lin, B. Guo, Swin transformer: Hierarchical vision transformer using shifted windows, in: Proceedings of the IEEE/CVF international conference on computer vision, 2021, pp. 10012–10022.
- [42] K. He, X. Zhang, S. Ren, J. Sun, Deep residual learning for image recognition, in: Proceedings of the IEEE conference on computer vision and pattern recognition, 2016, pp. 770–778.
- [43] Y. Liu, Y. Liu, C. Jiang, K. Lyu, W. Wan, H. Shen, B. Liang, Z. Fu, H. Wang, L. Yi, Hoi4d: A 4d egocentric dataset for category-level human-object interaction, in: Proceedings of the IEEE/CVF Conference on Computer Vision and Pattern Recognition, 2022, pp. 21013–21022.

- [44] Y. Tang, Y. Tian, J. Lu, J. Feng, J. Zhou, Action recognition in rgb-d egocentric videos, in: IEEE International Conference on Image Processing (ICIP), IEEE, 2017, pp. 3410–3414.
- [45] Z. Xu, D. Wu, C. Yu, X. Chu, N. Sang, C. Gao, Sctnet: Single-branch cnn with transformer semantic information for real-time segmentation, in: Proceedings of the AAAI Conference on Artificial Intelligence, Vol. 38, 2024, pp. 6378–6386.
- [46] R. Strudel, R. Garcia, I. Laptev, C. Schmid, Segmenter: Transformer for semantic segmentation, in: Proceedings of the IEEE/CVF international conference on computer vision, 2021, pp. 7262–7272.
- [47] D. Alexey, An image is worth 16x16 words: Transformers for image recognition at scale, arXiv preprint arXiv: 2010.11929 (2020).
- [48] B. Cheng, A. Schwing, A. Kirillov, Per-pixel classification is not all you need for semantic segmentation, Advances in neural information processing systems 34 (2021) 17864–17875.
- [49] B. Cheng, I. Misra, A. G. Schwing, A. Kirillov, R. Girdhar, Masked-attention mask transformer for universal image segmentation, in: Proceedings of the IEEE/CVF conference on computer vision and pattern recognition, 2022, pp. 1290–1299.